Communication

Peculiarities of γ-Al$_2$O$_3$ Crystallization on the Surface of h-BN Particles

Sergey N. Grigoriev [1], Elena A. Trusova [2], Asya M. Afzal [2], Thet Naing Soe [1], Alexandra Yu. Kurmysheva [1], Ekaterina Kuznetsova [1], Anton Smirnov [1,*] and Nestor Washington Solís Pinargote [1,*]

1   Laboratory of Electric Current Assisted Sintering Technologies, Moscow State University of Technology "STANKIN", Vadkovsky per. 1, 127055 Moscow, Russia
2   Baikov Institute of Metallurgy and Materias Science, RAS, Russian Academy of Sciences, Leninsky pr. 49, 119334 Moscow, Russia
*   Correspondence: a.smirnov@stankin.ru (A.S.); nw.solis@stankin.ru (N.W.S.P.);
     Tel.: +7-499-972-95-85 (N.W.S.P.)

Abstract: The main goal of the present work was to synthesize a composite consisting of h-BN particles coated with a γ-Al$_2$O$_3$ nanolayer. A method was proposed for applying nanocrystalline γ-Al$_2$O$_3$ to h-BN particles using a sol–gel technique, which ensures the chemical homogeneity of the composite at the nano level. It has been determined that during crystallization on the h-BN surface, the proportion of spinel in alumina decreases from 40 wt.% in pure γ-Al$_2$O$_3$ to 30 wt.% as a result of the involvement of the B^{3+} ions from the surface nitride monolayers into the transition complex. For comparison, nano-alumina was synthesized from the same sol under the same conditions as the composite. The characterization of the obtained nanostructured powders was carried out using TEM and XRD. A mechanism is proposed for the formation of a nanostructured γ-Al$_2$O$_3$@h-BN composite during the interaction of Al-containing sol and h-BN suspension in aqueous organic media. The resulting composite is a promising model of powdered raw materials for the development of fine-grained ceramic materials for a wide range of applications.

Keywords: h-BN; nano-alumina; sol–gel; γ-Al$_2$O$_3$@h-BN; nanostructures; crystallization on surface; chemical homogeneity of composites

1. Introduction

Hexagonal boron nitride (h-BN) has a layered crystalline structure similar to that of graphite, which gives it high lubricity and machinability, resulting in it also being known as "white graphite" [1]. In addition to these characteristics, h-BN has other equally important properties, such as excellent chemical resistance, thermal stability, and good thermal conductivity with no electrical conductivity [2–4], that make it a promising candidate for use in lubrication applications. In recent years, the joint combination of these properties has attracted the attention of many researchers to use h-BN as a solid lubricant, which can successfully perform the self-lubricating functions of ceramic tools [5–7].

Ceramic cutting tools, due to their unique properties (high hardness [8] and excellent resistance to high temperatures [9,10], corrosion resistance [11], and wear resistance [12]), are used in the machining of hard materials and superalloys, as they can withstand extreme machining conditions [13,14]. However, ceramic tools have high coefficients of friction and are sensitive to defects generated during dry cutting [15–17]. Therefore, the addition of h-BN to the ceramic matrix can significantly increase its lubricity. During the cutting process, h-BN particles can release, smear, and develop a thin lubricating film, which effectively reduces the coefficient of friction and wear rate of the tool–workpiece interface [18,19]. On the other hand, the softness of the h-BN particle decreases the overall mechanical properties of ceramic composites [20]. An effective solution to maintain the lubricating properties and ensure the preservation of the mechanical properties of the ceramic compound is the

formation of a protective layer on the surface of the h-BN particles [21–23]. For instance, Wu et al. [1] coated h-BN with a layer of Ni and showed that its addition to ceramic tools can avoid the negative effects on mechanical properties caused by the direct addition of h-BN. In another work, Chen et al. [24] compared to the addition of h-BN and h-BN@SiC to the Al_2O_3@TiC matrix and demonstrated that the inclusion of h-BN@SiC noticeably improved the mechanical properties and machinability of ceramic cutting tools.

Furthermore, it is known that the addition of h-BN leads to alumina toughening and prevents crack development, mainly by crack tip blunting [25–28]. Taking this fact into account and knowing that most ceramic cutting tools are made of alumina, it can be deduced that Al_2O_3 is an excellent material for h-BN coating. In addition, the coating of h-BN with Al_2O_3 can improve its interaction and dispersibility in the matrix of ceramic cutting tools [29]. This approach to improving the final product is common in many scientific fields [30–32].

We decided to combine the positive properties of h-BN and alumina in order to create a promising raw powder product for the sintering of fine-grained ceramics with improved properties. The potential market for such ceramics is almost comprehensive: from materials for miniaturized electronic devices operating under extreme conditions (high temperatures, vibration, mechanical stress) to blanks for cutting tools with improved performance characteristics (strength, wear resistance, durability). The creation of scientific foundations for the production technology of such materials will improve the accuracy of measuring instruments and cutting tools, optimize the costs of the reconstruction of existing industries, and increase the efficiency of production in general [33].

In this work, a mechanism for the formation of crystalline alumina on the surface of crystals is proposed, which explains a simple, economic, and fast method of obtaining h-BN@ γ-Al_2O_3 particles. In this method, nanocrystalline alumina can be deposited on h-BN nanocrystals using the sol–gel method. Furthermore, the influence of the h-BN crystal lattice on the morphology of Al_2O_3 and the proportion and syngony of spinel in its composition were also studied. The synthesized powders were characterized using X-ray diffraction (XRD) and transmission electron microscopy (TEM).

2. Materials and Methods

2.1. Preparation of Nanostructured γ-Al_2O_3@h-BN Powder

A nanolayer of γ-Al_2O_3 was deposited using the sol–gel method [34] on commercially available h-BN powder with an average particle size of 70 nm. The two-step γ-Al_2O_3 deposition process included obtaining a suspension of h-BN powder in a water–alcohol mixture with deionized water and isopropanol at a volume ratio of 2:1. The details of the purity and manufacturers of the reagents used are provided in Table 1. For the synthesis of the Al-containing sol, an aqueous solution of aluminum nitrate nonahydrate ($Al(NO_3)_3 \cdot 9H_2O$) at a concentration of 0.4 M was prepared. Then, in order to form and stabilize the sol, the monoethanolamine (MEA) was added to the $Al(NO_3)_3$ solution at an MEA/Al molar ratio of 3:1.

Once the h-BN suspension and the Al-containing sol were prepared, they were mixed through stirring (at 250 rpm) on a magnetic stirrer for 20–25 min and heated to 60–65 °C. Then, the mixture was evaporated with constant stirring at a temperature of 95–98 °C until a viscous mass was obtained. After that, the resulting mass was transferred into a porcelain cup and placed in a furnace, where heat treatment was carried out at 900 °C for 1 h. As a result, a fine white powder was synthesized with an h-BN content of 1.20 ($\pm$0.06) wt.%.

Table 1. Purity and manufacturers of the reagents used.

Raw Materials	Purity	Manufacturer, Country
h-BN powder	>99.00%	Plasmotherm Ltd., Moscow, Russia
Aluminum nitrate nonahydrate $Al(NO_3)_3 \cdot 9H_2O$	>97.00%	GOST 3757-75, ChimMed, Moscow, Russia
Monoethanolamine	99.40%	TU 2632-094-44493179-04, EKOS-1, Moscow, Russia
Isopropanol	99.99%	CAS 67-63-0, Sigma-Aldrich, Darmstadt, Germany
Deionized water	specific conductivity < 1 mcm/cm	Raifil water purification system, GOST 6709-72

2.2. Characterization of Synthesized Powders

An X-ray diffractometer (SHIMADZU XRD-6000, Shimadzu, Japan) with monochromatic copper radiation ($\lambda K\alpha = 1.54178$ Å) and Zeeman–Bolin focusing was used to analyze the phase composition of the as-prepared particles. The determination of the phase composition was carried out using JCPDS cards. The studies were performed at room temperature and under normal atmospheric pressure. The average crystallite size was calculated using the Rietveld method, which uses an iterative procedure to minimize the experimental diffraction pattern deviations from the calculated data. Transmission electron microscopy (TEM) studies of obtained pure γ-Al_2O_3 were carried out with the use of an LEO-912 AB OMEGA (Leo Elektronenmikroskopie, Oberkochen, Germany) electron microscope operating at 100 kV.

3. Results and Discussion

After MEA was added to the 0.4 M aqueous solution of aluminum nitrate, an Al-containing sol was formed as a result of the interaction of hydrolyzed MEA molecules and $Al(NO_3)_3$, as shown in Figure 1a. As is known, the hydrolysis of aluminum nitrate occurs in steps, and Figure 1a shows its first stage [34]. The quaternary ammonium ion and the triply charged nitrate anion were the centers of interaction between the MEA and aluminum nitrate. At an MEA/$Al(NO_3)_3$ molar ratio of 3:1, as a result of complexation, a sol with the overall formula of AlR_3 was formed, and further, it was adsorbed on the surface of the crystalline h-BN particles. During the heat treatment (900 °C) of the resulting mixed colloid, the sol → gel transition (Figure 1b) occurs on the surface of h-BN crystalline particles. In this case, as a result of the polycondensation reaction, which was implemented at the first stage of heat treatment, an oligomeric gel was formed. The latter decomposed upon calcination in the air at 900 °C; this led to the crystallization of γ-Al_2O_3 on the centers of the surface of h-BN particles, which were formed earlier during the adsorption of the Al-containing sol on them (Figure 2).

The organic component of the gel was removed as water vapor and carbon and nitrogen oxides during the thermal degradation of the oligomeric gel (Figures 1b and 2). The use of a high mass ratio of Al-containing sol and h-BN made it possible to create γ-Al_2O_3 shells on the particles of the latter.

Figure 3 shows the XRD patterns of a prepared γ-Al_2O_3@h-BN composite and pure γ-Al_2O_3, obtained from the same sol (inset). A comparison of alumina crystallites formed during the heat treatment of the Al-containing sol and alumina crystallites formed on the h-BN surface shows some differences in their qualitative and quantitative compositions.
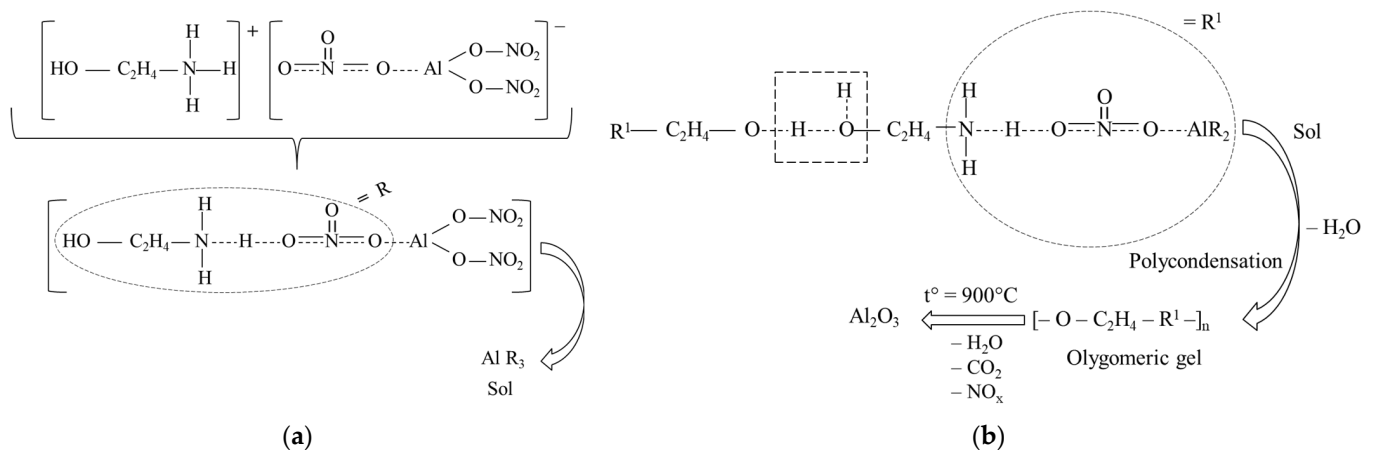
Figure 1. Schemes of (**a**) the formation of the Al-containing sol; and (**b**) the heat treatment of Al-containing sol within a wide temperature range, up to 900 °C, which includes the polycondensation of the complex sol and subsequent thermal destruction of the formed oligomeric gel, leading to the formation of nanocrystalline γ-Al$_2$O$_3$.
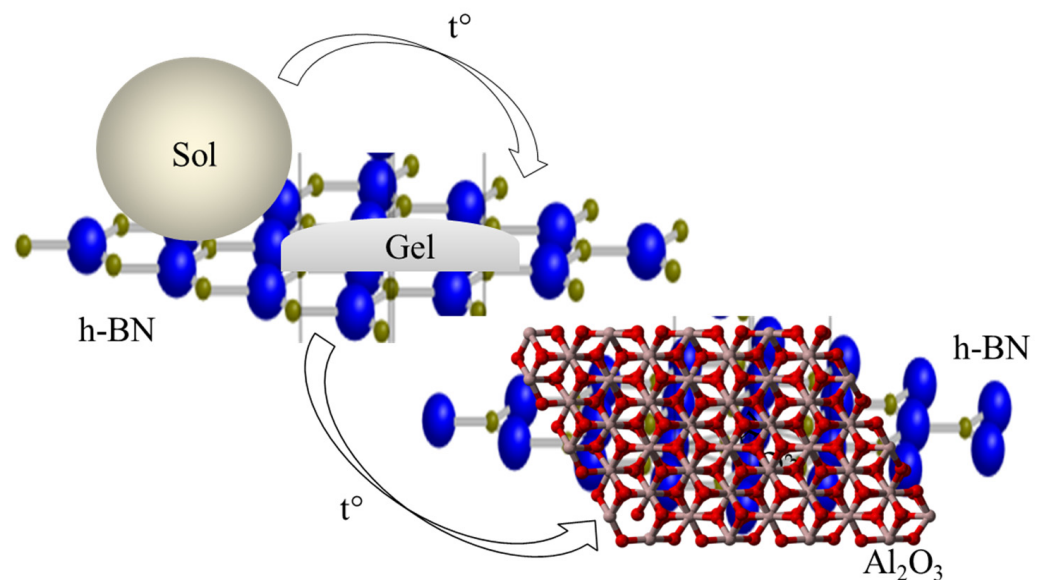

Figure 2. Scheme of the formation of the γ-Al$_2$O$_3$ crystal lattice on the surface of h-BN particles.

The pure γ-Al$_2$O$_3$ consisted of two syngony species, cF56 and cF8, assigned according to card Nos. 10-0425 and 75-0278 of the ICDD PDF-2 2003 database, respectively. In Figure 3, the syngony species cF56 and cF8 are indicated by the symbols * and **, respectively. Both modifications correspond to the space group Fm3m, whose anions form a face-centered cubic lattice. The medium sizes of the crystallites from the cF56 and cF8 modifications, as calculated using the Rietveld method, were 3 and 7 nm, respectively. The proportions of alumina in the cF56 and cF syngony species were 60 and 40 wt.%, respectively, and thus, the weight ratio of alumina in the cF56 and cF8 syngony species was 1.5.

According to the TEM data, alumina consisted of cubic nanocrystals less than 10 nm in size (Figure 4a), which is in good agreement with the XRD data. At the same time, the high dispersity of crystallites with cubic syngony was shown in the electron diffraction pattern (Figure 4a, inset).
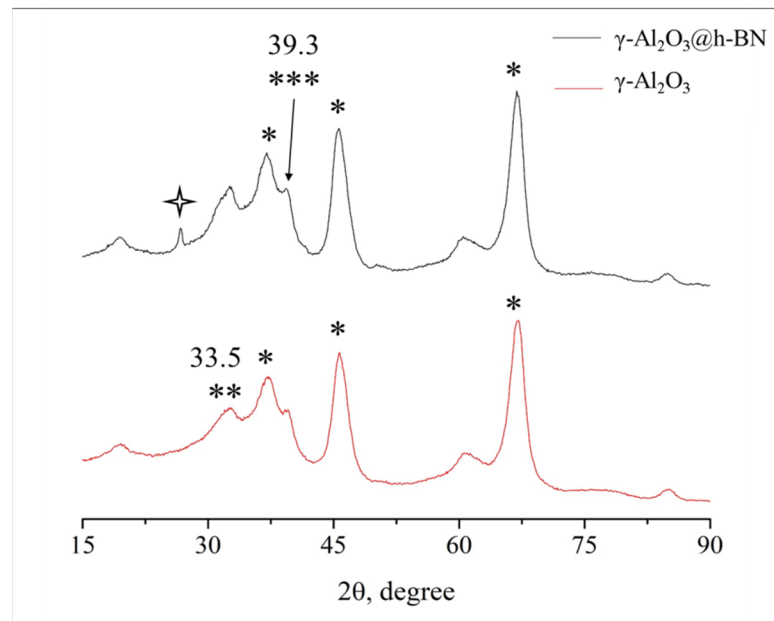
Figure 3. XRD patterns for the γ-Al$_2$O$_3$/h-BN composite and pure γ-Al$_2$O$_3$, obtained from the same sol. *—γ-Al$_2$O$_3$ cF56 (card № 10-0425 ICDD PDF-2 2003); **—γ-Al$_2$O$_3$ cF8 (card № 75-0278 ICDD PDF-2 2003); ***—γ-Al$_2$O$_3$ cF16 [24,25]; ✦—h-BN.
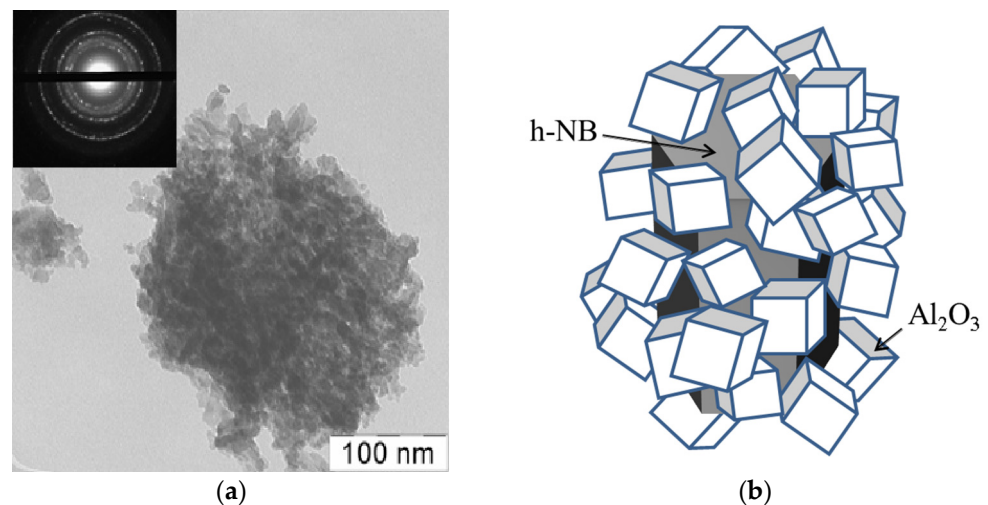

Figure 4. TEM image for pure nano-alumina and electron diffraction (inset) (**a**); scheme of shell formation from γ-Al$_2$O$_3$ on h-BN crystalline particles (**b**).

The XRD data for the composite obtained through the deposition of γ-Al$_2$O$_3$ on the h-BN powder from an Al-containing sol differed from the data for pure alumina, as shown in Figure 3. As in the case of pure γ-Al$_2$O$_3$, most of the alumina (70 wt.%) was crystallized in the form of the cF56 syngony with an average crystallite size of less than 3 nm, as calculated using the Rietveld method. The rest of the alumina was crystallized in the form of the cF16 syngony with an average crystallite size of 8 nm. In Figure 3, the syngony species cF16 is indicated by the symbol ***, and it was assigned according to the information presented in [34,35]. Thus, it can be noted that when the crystallization of alumina occurred in the presence of h-BN, the formation of the cF56 syngony occurred more actively, apparently due to the fact that the process occurred on the h-BN surface. At the same time, γ-Al$_2$O$_3$ appeared in the cF16 system, which was a spinel like the cF8 system in pure γ-Al$_2$O$_3$.

A comparison of the crystal lattice parameters of two types of syngony showed that the cF56 lattice was deformed during the formation of γ-Al_2O_3 on the surface of h-BN crystals, and thus led to the formation of a spinel with the cF16 syngony. The crystal lattice parameter of the cF16 syngony was equal to 3.951 Å, which differs significantly from the corresponding parameter for the spinel cF8, which was equal to 4.096 Å.

In previous works [34,35], a similar phenomenon was observed in the case of the formation of the $MgAl_6O_{10}$ spinel. During sol–gel synthesis, the covalent interaction of the Al–organic complex with a cation, different from Al^{3+} in size and charge, led to the formation of a spinel with the syngony cF16.

Mild conditions for the synthesis of the γ-Al_2O_3@h-BN composite cannot promote the incorporation of B^{3+} ions into the spinel crystal lattice; therefore, it can be assumed that its formation occurs through a surface complex centered on the B^{3+} ion. Apparently, the thermal destruction of the oligomeric gel (Figure 1a), and the subsequent crystallization of alumina on the h-BN surface (Figure 1b), proceed through the formation of a surface complex with the participation of the B^{3+} ion of the surface monolayers of BN crystallites. Figure 4b schematically shows the structure of the nanostructured composite obtained as a result of the deposition of γ-Al_2O_3 nanocrystals to h-BN particles.

Thus, we have shown that the direction of alumina crystallization from an oligomeric Al-containing gel on the surface of h-BN particles was determined by B^{3+} ions, which acted as centers of spinel crystallization. In this case, the presence of h-BN promoted a more intense formation of γ-Al_2O_3 and an increase in its yield compared to crystallization from a single Al-containing sol. As a result, it was possible to obtain a more homogeneous γ-Al_2O_3 phase with a reduced content of spinel.

4. Conclusions

Thus, we have proposed a simple, economic, and quick method of obtaining an h-BN@γ-Al_2O_3 powder composite with high chemical and phase composition homogeneity, which is intended for sintering special types of ceramics. It was shown that during alumina crystallization on the h-BN surface, the fraction of spinel in alumina decreased from 40 wt.% in pure γ-Al_2O_3 to 30 wt.% as a result of the involvement of B^{3+} ions in the nitride surface monolayers to the transition complex. A mechanism has been proposed for the formation of a nanostructured composite γ-Al_2O_3@h-BN during the interaction of Al-containing sol and h-BN suspension in organic-aqua media, according to which, alumina crystallization occurred on the B^{3+} centers. The use of the proposed method for obtaining the h-BN@γ-Al_2O_3 composite is promising for the creation of new technologies for the production of raw materials for a wide range of purposes.

Author Contributions: Conceptualization, E.A.T. and A.M.A.; methodology, E.A.T. and A.M.A.; validation, E.A.T. and A.M.A.; formal analysis, E.A.T., A.M.A. and A.S.; investigation, E.A.T., A.M.A. and A.Y.K.; resources, E.A.T., A.M.A. and N.W.S.P.; data curation, E.A.T., T.N.S. and A.M.A.; writing—original draft preparation, E.A.T., N.W.S.P. and A.S.; writing—review and editing, E.A.T., N.W.S.P., A.S., A.Y.K. and E.K.; visualization, E.A.T., A.M.A., T.N.S. and E.K.; supervision, E.A.T.; project administration, N.W.S.P. and S.N.G.; funding acquisition, S.N.G. All authors have read and agreed to the published version of the manuscript.

Institutional Review Board Statement: Not applicable.

Informed Consent Statement: Not applicable.

Data Availability Statement: The data described in this article are openly available in previous works.

Conflicts of Interest: The authors declare no conflict of interest.

References

1. Wu, G.; Xu, C.; Xiao, G.; Yi, M.; Chen, Z.; Chen, H. An advanced self-lubricating ceramic composite with the addition of core-shell structured h-BN@Ni powders. *Int. J. Refract. Metal Hard Mater.* **2018**, *72*, 276–285. [CrossRef]
2. Bilaç, O.; Duran, C. Al_2O_3/glass/hBN composites with high thermal conductivity and low dielectric constant for low temperature cofired ceramic applications. *J. Asian Ceram. Soc.* **2021**, *9*, 283–290. [CrossRef]
3. Chiang, T.H.; Hsieh, T.-E. Study of encapsulation resin containing hexagonal boron nitride (hBN) as inorganic filler. *J. Inorg. Organomet. Polym. Mater.* **2006**, *16*, 175–183. [CrossRef]
4. Tian, Z.; Wang, Y.; Zhang, Z.; Duan, X.; Jia, D.; Wu, S. The effects of holding time on grain size, orientation degree and properties of h-BN matrix textured ceramics. *Mater. Chem. Phys.* **2020**, *248*, 122916. [CrossRef]
5. Kuang, W.J.; Zhao, B.; Yang, C.Y.; Ding, W.F. Effects of h-BN particles on the microstructure and tribological property of self-lubrication CBN abrasive composites. *Ceram. Int.* **2020**, *46*, 2457–2464. [CrossRef]
6. Cao, T.K.; Zhu, Z.B.; Liu, Y.J. Preparation of a self-lubricating Cu/h-BN coating on cemented carbide. *Adv. Mater. Sci. Eng.* **2018**, *2018*, 8150791. [CrossRef]
7. Mahathanabodee, S.; Palathai, T.; Raadnui, S.; Tongsri, R.; Sombatsompop, N. Dry sliding wear behavior of SS316L composites containing h-BN and MoS2 solid lubricants. *Wear* **2014**, *316*, 37–48. [CrossRef]
8. Volosova, M.; Grigoriev, S.; Metel, A.; Shein, A. The Role of Thin-Film Vacuum-Plasma Coatings and Their Influence on the Efficiency of Ceramic Cutting Inserts. *Coatings* **2018**, *8*, 287. [CrossRef]
9. Grigor'ev, S.N.; Kuzin, V.V. Prospects for tools with ceramic cutting plates in modern metal working. *Glass Ceram.* **2011**, *68*, 253–257. [CrossRef]
10. Grigoriev, S.N.; Kozochkin, M.P.; Porvatov, A.N.; Volosova, M.A.; Okunkova, A.A. Electrical discharge machining of ceramic nanocomposites: Sublimation phenomena and adaptive control. *Heliyon* **2019**, *5*, e02629. [CrossRef]
11. Grigoriev, S.N.; Vereschaka, A.A.; Fyodorov, S.V.; Sitnikov, N.N.; Batako, A.D. Comparative analysis of cutting properties and nature of wear of carbide cutting tools with multi-layered nano-structured and gradient coatings produced by using of various deposition methods. *Int. J. Adv. Manufact. Technol.* **2017**, *90*, 3421–3435. [CrossRef]
12. Kuzin, V.V.; Grigoriev, S.N.; Volosova, M.A. The role of the thermal factor in the wear mechanism of ceramic tools: Part 1. Macrolevel. *J. Frict. Wear* **2014**, *35*, 505–510. [CrossRef]
13. Kumar, A.S.; Durai, A.R.; Sornakumar, T. Wear behaviour of alumina based ceramic cutting tools on machining steels. *Tribol. Int.* **2006**, *39*, 191–197. [CrossRef]
14. Tian, X.; Zhao, J.; Zhao, J.; Gong, Z.; Dong, Y. Effect of cutting speed on cutting forces and wear mechanisms in high-speed face milling of Inconel 718 with Sialon ceramic tools. *Int. J. Adv. Manuf. Technol.* **2013**, *69*, 2669–2678. [CrossRef]
15. Wang, R.; Li, W. Determining fracture strength and critical flaw of the ZrB_2–SiC composites on high temperature oxidation using theoretical method. *Compos. B Eng.* **2017**, *129*, 198–203. [CrossRef]
16. Ariharan, S.; Nisar, A.; Balaji, N.; Aruna, S.; Balani, K. Carbon nanotubes stabilize high temperature phase and toughen Al_2O_3-based thermal barrier coatings. *Compos. B Eng.* **2017**, *124*, 76–87. [CrossRef]
17. Liu, Y.; Fu, Q.; Zhao, F.; Sun, G.; Li, H. Internal friction vs. thermal shock in C/C composites. *Compos. B Eng.* **2016**, *106*, 59–65. [CrossRef]
18. Wu, J.; Wang, H.; Wang, C.; Zhang, Z.; Tang, Y.; Hou, Z.; Wan, S.; Wu, D.; Tan, Z.; Ouyang, X. High-Pressure synthesis of Al_2O_3-cBN-hBN Self-lubricating ceramic. *Mater. Des.* **2022**, *217*, 110638. [CrossRef]
19. Smirnov, A.; Seleznev, A.; Solís Pinargote, N.W.; Pristinskiy, Y.; Peretyagin, P.; Bartolomé, J.F. The Influence of Wire Electrical Discharge Machining Cutting Parameters on the Surface Roughness and Flexural Strength of ZrO_2/TiN Ceramic. Nanocomposites Obtained by Spark Plasma Sintering. *Nanomaterials* **2019**, *9*, 1391. [CrossRef]
20. Akhtar, S.S. A critical review on self-lubricating ceramic-composite cutting tools. *Ceram. Int.* **2021**, *47*, 20745–20767. [CrossRef]
21. Ding, X.; Luo, L.; Huang, L.; Luo, G.; Zhu, X.; Ji-Gui, C.; Wu, Y.C. Preparation of TiC/W core-shell structured powders by one-step activation and chemical reduction process. *J. Alloys Compd.* **2015**, *619*, 704–708. [CrossRef]
22. Zhang, L.; Ren, Y.; Peng, S.; Guo, D.; Wen, S.; Luo, J.; Xie, G. Core-shell nanospheres to achieve ultralow friction polymer nanocomposites with superior mechanical properties. *Nanoscale* **2019**, *11*, 8237–8246. [CrossRef] [PubMed]
23. Carabata, A.L.; Meijerink, M.J.; Brouwer, J.C.; Kelder, E.M.; van Ommen, J.R.; van der Zwaag, S.; Sloof, W.G. Protecting the $MoSi_2$ healing particles for thermal barrier coatings using a sol-gel produced Al_2O_3 coating. *J. Eur. Ceram. Soc.* **2018**, *38*, 2728–2734. [CrossRef]
24. Chen, H.; Xu, C.; Xiao, G.; Chen, Z.; Wu, Z.; Yi, M. Investigation of Al_2O_3/TiC ceramic cutting tool materials with the addition of SiC-coated h-BN: Preparation, mechanical properties, microstructure and wear resistance. *Int. J. Mater. Res.* **2016**, *107*, 735–740. [CrossRef]
25. Popov, O.; Vishnyakov, V.; Fleming, L.; Podgurskiy, M.; Blunt, L. Reaction Sintering of Biocompatible Al_2O_3−hBN Ceramics. *ACS Omega* **2022**, *7*, 2205–2209. [CrossRef] [PubMed]
26. Yang, S.F.; Yang, L.Q.; Jin, Z.H.; Guo, T.W.; Wang, L.; Liu, H.C. New nano-sized Al_2O_3-BN coating 3Y-TZP ceramic composites for CAD/CAM−produced all-ceramic dental restorations. Part I. Fabrication of powders. *Nanomedicine* **2009**, *5*, 232–239. [CrossRef]
27. Li, Y.; Qiao, G.; Jin, Z. Mahcinable Al_2O_3/BN ceramics with strong mechanical properties. *Mater. Res. Bull.* **2002**, *37*, 1401–1409. [CrossRef]

28. Kusunose, T.; Kim, Y.-H.; Sekino, T.; Matsumoto, T.; Tanaka, N.; Nakayama, T.; Niihara, K. Fabrication of Al_2O_3/BN nanocomposites by chemical processing and their mechanical properties. *J. Mater. Res.* **2005**, *20*, 183–191. [CrossRef]

29. Fernandez-Garcia, E.; Gutierrez-Gonzalez, C.F.; Peretyagin, P.; Solis, W.; Lopez-Esteban, S.; Torrecillas, R.; Fernandez, A. Effect of yttria–titanium shell–core structured powder on strength and ageing of zirconia/titanium composites. *Mater. Sci. Eng. A* **2015**, *646*, 96–100. [CrossRef]

30. Zaghloul, M.M.Y.; Zaghloul, M.Y.M.; Zaghloul, M.M.Y. Experimental and modeling anal-ysis of mechanical-electrical behaviors of polypropylene composites filled with graphite and MWCNT fillers. *Polym. Test.* **2018**, *63*, 467–474. [CrossRef]

31. Fuseini, M.; Zaghloul, M.M.Y. Inves-tigation of Electrophoretic Deposition of PANI Nano fibers as a Manufacturing Technolo-gy for corrosion protection. *Progr. Org. Coat.* **2022**, *171*, 107015. [CrossRef]

32. Zaghloul, M.M.Y.M. Mechanical proper-ties of linear low-density polyethylene fire-retarded with melamine polyphosphate. *J. Appl. Polym. Sci.* **2018**, *135*, 46770. [CrossRef]

33. Hung, C.-C.; Hurst, J.; Santiago, D.; Lizcano, M.; Kelly, M. Highly Thermally Conductive Hexagonal Boron Nitride/Alumina Composite Made From Commercial Hexagonal Boron Nitride. *J. Am. Ceram. Soc.* **2016**, *100*, 515–519. [CrossRef]

34. Khrushcheva, A.A. Sol-Gel Synthesis of Composite Nanoparticles Based on Aluminum, Cerium and Zirconium Oxides. Ph.D. Thesis, Baikov Institute of Metallurgy and Materias Science, RAS, Moscow, Russia, 2016.

35. Trusova, E.A.; Khrushcheva, A.A.; Kotsareva, K.V.; Vokhmintcev, K.V. The laboratory technology for nanodispersed raw products and fine-grained ceramics. In Proceedings of the 2014 World Congress on Advances in Civil, Environmental and Materials Research, Busan, Korea, 24–28 August 2014; M4E.4.MR363_231F-2; 10p.